

DESY Summer Student Programme Report
Point resolution of a time projection chamber with
GEM readout

Nils Kanning*
Supervisor: Ralf Diener

September 16, 2008

Contents

1	Introduction	2
2	Theory	2
2.1	Physical Principles	2
2.2	Time Projection Chamber	4
3	Experimental Setup and Data Reconstruction	7
3.1	MediTPC	7
3.2	MultiFit	8
3.3	ROOT Analysis Scripts	16
4	Analysis and Results	18
4.1	Track Reconstruction	18
4.2	Point Resolution	20
4.3	Pad Response Correction	26
5	Results and Outlook	36

*Fakultät für Physik, Universität Göttingen

1 Introduction

During my stay as a Summer Student at DESY in Hamburg from Juli 23 until September 16 I worked with the FLC/TPC group. This group does research on a *Time Projection Chamber* (TPC) for the *International Linear Collider* (ILC).

In contrast to the *Large Hadron Collider* (LHC) which starts operation this fall and in which protons are accelerated in a circular orbit, at the future ILC electrons and positrons, accelerated along a straight path, will collide. The advantage of the ILC is that the initial state of the reaction is well known. So high precision measurements are possible, which demand for a highly efficient and precise detector. One possibility for the main tracker of such a detector is a TPC. This detector component makes it possible to reconstruct the tracks of charged particles. To achieve the high efficiency and precision a good resolution of the track reconstruction is essential. Because the momentum of the particles can be reconstructed using the track data, the track resolution directly affects the momentum resolution of the detector.

One research topic of the DESY FLC/TPC group – this was also the main subject of my work – are studies regarding the resolution of the track reconstruction. These studies are performed using data taken with a TPC prototype at the laboratory at DESY.

In this report first an introduction about the physical principles and the operation of a TPC will be given. Then a description of the test setup at DESY and the software and algorithms used to analyze the data recorded with this prototype follows.

2 Theory

The operation of a TPC is based on the free electrons and ions created due to ionization if a charged particle passes through a gas volume. Consequently we have to discuss how these electrons are created and how they behave.

2.1 Physical Principles

2.1.1 Interaction of Particles with Matter

If a particle passes through a gas volume there are especially two kinds of interactions with the gas molecules: inelastic collisions with an electron of a gas molecule and elastic scattering at the nucleus of a gas molecule.

During these processes the particle loses energy. For heavy particles, e.g. muons, this loss is nearly complete due to the inelastic collisions. The atoms are excited or ionized. The measurement of the liberated electrons will be the basis of the TPC operation.

A quantum mechanical calculation offers the average energy loss of a particle passing through a gas volume per unit path length as a function of the particle's velocity v :

$$-\left\langle \frac{dE}{dx} \right\rangle = 2\pi N_a r^2 m c^2 \rho^2 \frac{Z}{A} \frac{z^2}{\beta^2} \left[\ln \left(\frac{2mc\gamma^2 v^2 W_{\max}}{I^2} \right) - 2\beta^2 \right] \quad (1)$$

This formula is well known as the *Bethe-Bloch equation*¹[1]. The symbols used are the Avogadro constant N_a , the classical radius of the electron r , the mass of the electron m , the density of the gas ρ , the atomic number of the gas Z , the atomic weight of the gas A , the charge of the particle z in units of the elementary

¹For convenience we omit two correction terms.

charge e , the mean excitation potential I , the maximal energy transferred at a single collision W_{\max} , the speed of light in vacuum c and the two quantities $\beta = v/c$ and $\gamma = \sqrt{1 - \beta^2}^{-1}$.

Since the loss of energy of the particle is a statistical process there are fluctuations from the above value. It turns out that in a gas the energy loss follows a landau distribution.[1]

2.1.2 Drift and Diffusion of Electrons and Ions in Gases

According to the processes described so far, after the passage of a particle through gas there are electrons and ions left.

The movement of a single one of these electrons² is described by the *Langevin equation*[2]:

$$m \frac{d\vec{v}}{dt} = e\vec{E} + e(\vec{v} \times \vec{B}) + \vec{Q}(t)$$

Here $\vec{Q}(t)$ is a stochastic force term due to the collisions with the surrounding gas molecules. Furthermore the electric field \vec{E} and the magnetic field \vec{B} are introduced.

The stationary solution $\vec{v}_D = \langle v \rangle$ of the above equation is called *drift velocity* and represents the mean velocity of the electrons:

$$\vec{v}_D = \frac{\mu E}{1 + \omega^2 \tau^2} \left[\hat{E} + \omega \tau (\hat{E} \times \hat{B}) + \omega^2 \tau^2 (\hat{E} \hat{B}) \hat{B} \right] \quad (2)$$

Here τ is the mean time between two collisions and $\vec{\omega} = e\vec{B}/m$ and also $\mu = e\tau/m$. Furthermore the caret indicates a unit vector.

The Langevin equation can be used to calculate the mean position $\langle x(t) \rangle$ of an ensemble of electrons. The equation also shows that the width of the distribution $\sigma(t)$ of the positions $x(t)$ increases with time. The spreading of the ensemble is called *diffusion* and we define the *diffusion coefficient* to be³:

$$D = \frac{\sigma(t)}{\sqrt{t} v_D} \quad (3)$$

This coefficient turns out to be independent of time. It depends on the gas mixture and the \vec{E} and \vec{B} field.

It can also be shown that in the presence of a magnetic field \vec{B} the diffusion perpendicular to the field decreases.

2.1.3 Avalanche Multiplication

The charge of the number of electrons n_0 created during the primary ionization process described above is generally not enough to be measured accurately.

Therefore their energy is increased by applying an external electric field \vec{E} . The electrons now gain energy until they can ionize further molecules themselves, which leads to a avalanche multiplication [1] of the number of available free electrons n :

$$n = n_0 \exp(\alpha x)$$

Here α is the *first Townsend coefficient* and x is the length of the path of the primary electrons.

²and ions – which will be omitted from now on

³Strictly speaking the diffusion coefficient depends on the direction: $\sigma(t)$ is the spread of $x(t)$ perpendicular to this direction and v_D is the component of the drift velocity in this direction.

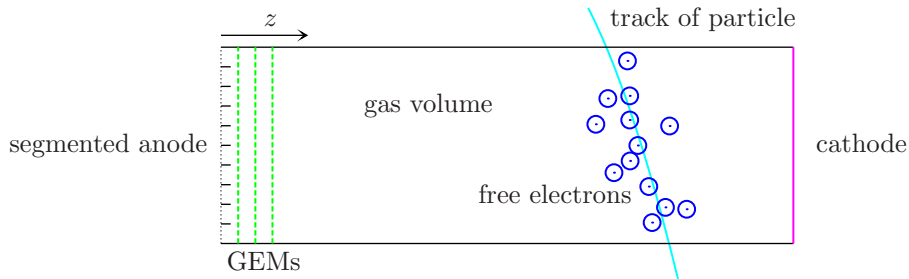


Figure 1: Schematic image of a TPC

2.2 Time Projection Chamber

The *Time Projection Chamber* (TPC) is a particle detector capable of reconstructing the three-dimensional track of a particle. It was invented in 1975 by D.R. Nygren[3]. Using a TPC in a magnetic field, the momentum of a charged particle can be identified. Furthermore, the deposited energy $\langle dE/dx \rangle$ of the particle can be measured with a TPC. The latter will not be discussed in this report.

2.2.1 Principle of Operation

A typical TPC consists of a large cylinder⁴ filled with gas (see Fig. 1). Between the two end caps of the cylinder a high voltage is applied, causing a constant electric field \vec{E} along the longitudinal axis of the cylinder. In most cases this system is placed in a magnetic field \vec{B} that is parallel to the electric field.

If a charged particle traverses the gas volume it loses energy according to the Bethe-Bloch equation (Eq. 1) and the gas molecules are ionized along the track of the particle. Due to the drift field the created electrons move towards the positively charged end cap (anode) with a constant velocity (Eq. 2).

Consequently the positions where these electrons reach the anode represent a two-dimensional projection of the particle track on the end cap. This projection is parametrized using (r, ϕ) or (x, y) . The longitudinal – or z – components of the track depend linearly on the time difference between the arrival of the electrons at the anode and the passage of the original particle, which is measured by an independent detector.

The positively charged ions, that are also created by the ionization process, are not used in this analysis. Rather they are obstructive because they can disturb the constant electric field.

2.2.2 Gas Amplification and Readout System

In order to determine the position of the electrons, the anode is realized as a segmented pad plane.

Since the signal of the primary ionization is not sufficient for an accurate measurement, it has to be amplified. In the past so called *Multiwire Proportional Chambers* (MWPC) have been used for this purpose.[13] Today concepts such as *Gas Electron Multipliers* (GEM)⁵ are often used. A GEM is a thin insulating foil with a conducting layer on the top and bottom side and with a regular pattern of holes (see Fig. 2). One or several of these GEMs are placed in a small distance in front of

⁴usually with a length of several meters

⁵introduced in 1997 by F. Sauli[5]

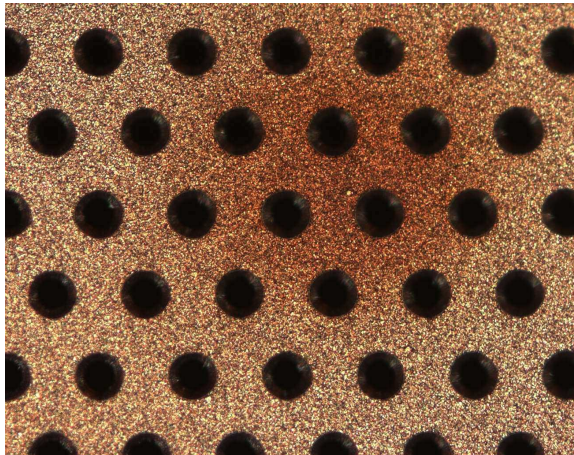


Figure 2: Microscopic image of a GEM showing the hole pattern; the distance between the centers of two holes is about $140\ \mu\text{m}$

the pad plane with a relative large potential difference between the top and bottom side of each GEM (see Fig. 1).

Because of this voltage, there is a large electric field inside the GEM holes. Consequently the electrons can gain enough energy to start secondary ionization which causes an avalanche multiplication.

Using this technique an amplification factor in the order of 10^4 can be achieved. These signals are sufficiently strong to be read out at the pad plane.

2.2.3 Point Resolution

During the data analysis, the signals from the pads are grouped to several points belonging to a track. The theoretical transverse resolution of these points σ_T depends on the spread of a signal due to transverse diffusion (Eq. 3). Apart from this diffusion, the GEMs also cause a constant spread of the electron distribution. This effect is called *defocusing* and is described by a constant term σ_0 . Due to effects described in [13] for the resolution the diffusion coefficient and the defocusing constant have to be modified and constants D' and σ'_0 are used instead. The resolution is then given by⁶:

$$\sigma_T = \sqrt{D'^2 z + \sigma_0'^2} \quad (4)$$

In practice this formula gives a lower limit for the point resolution σ_T because some electrons might have a certain initial velocity right after the ionization, which does not agree with the approach of assuming a constant drift velocity. Furthermore the point resolution is decreased by the readout, especially by the finite pad size. Consequently in practice the available point resolution σ_T has to be determined experimentally. This will be discussed later.

Because of the magnetic field \vec{B} , the track of the particle is a helix which, projected on the (r, ϕ) plane is a circle of radius R or respectively of curvature $\Omega = 1/R$. The error of the curvature is given as a function of the point resolution σ_T by the *Gluckstern formula*⁷[4]:

$$\sigma_\Omega = \frac{\sigma_T}{L^2} \sqrt{\frac{720(N-1)^3}{(N-2)N(N+1)(N+2)}}$$

⁶We introduce the notation $z \equiv \langle z \rangle = t v_D$.

⁷where N is the number of points belonging to the track and L the length of the track

Using the Lorentz force the transverse momentum p_T of a particle of charge q can be calculated to be:

$$p_T = \left| \frac{qB}{\Omega} \right|$$

This allows the computation of the relative transverse momentum resolution:

$$\frac{\sigma_{p_T}}{p_T} = \frac{\sigma_T}{L^2} \frac{p_T}{|qB|} \sqrt{\frac{720(N-1)^3}{(N-2)N(N+1)(N+2)}}$$

Since the momentum resolution depends linearly on the point resolution, a small σ_T is essential to be able to achieve the precision necessary for the measured physics processes.

Therefore the study of the point resolution is one of the main topics of this report.



Figure 3: Photo of the MediTPC prototype (left) and the MediTPC inside the magnet (right)

3 Experimental Setup and Data Reconstruction

3.1 MediTPC

The data used in the following analysis was measured with a TPC prototype at DESY – the *MediTPC*[6]. Pictures of the chamber are shown in Fig. 3.

3.1.1 Properties and Settings of the Measurement Runs

This chamber has a length of 800 mm and a diameter of 270 mm. However the sensitive volume is limited by the size of the pad plane which is generally smaller than the end caps of the cylinder.

The sensitive part of the pad plane consists of 48 columns and 12 rows. Each pad has a size of $1.12 \times 6.835 \text{ mm}^2$. A spacing of the pads causes a pitch of $1.27 \times 6.985 \text{ mm}^2$. For comparison also measurements with a pad plane composed of 24 columns and 6 rows and a pitch of $2.2 \times 6.2 \text{ mm}^2$ have been used. Both pad planes have a non-staggered layout.⁸

The TPC is filled with P5 gas, a mixture of 95% Ar and 5% CH₄.

The whole prototype is placed inside a superconducting magnet offering a field strength of up to 5.25 T. The measurements analyzed in the context of this work were performed using magnetic fields of either 1 T, 3 T or 4 T. The electric field in the gas volume has an amplitude of 92 V/cm.

There are three GEM layers placed in front of the pad plane. The signals on the pads are amplified with preamplifiers which contain pulse shapers. Then the signals are digitalized using *Time Projection Digitizers* (TPD) and written to disk in the *LCIO file format*[11], which has been specifically designed for the ILC software framework.

For this setup theoretical values of the transverse diffusion coefficient D and the defocusing constant σ_0 are available from a GARFIELD simulation[14]. These values are summarized in Tab. 1 and can, except for the 3 T values, also be found in [8].

⁸This means that the pads are aligned in x and y direction.

B [T]	D [$\sqrt{\text{mm}}$]	σ_0 [mm]
1	0.0495	0.477
3	0.0174	0.396
4	0.0139	0.375

Table 1: Transverse diffusion coefficient D and defocusing constant σ_0

3.1.2 Cosmic Muons and Triggers

In a big particle detector a TPC is usually placed in a way that it encloses the interaction point of a particle collider. In this case the tracks of the particles created in the collisions can be recorded.

In contrast the MediTPC measures the tracks of cosmic muons. Two scintillators are attached below and above the coil of the magnet. These scintillators trigger if a muon passes through. In case of a coincidence of both trigger signals the event is recorded to disk. This results in an event rate of about 1 Hz depending on the rate of the muons and the speed of the readout electronics.

3.2 MultiFit

After a measurement run, which typically contains several ten thousand events, the particle tracks have to be reconstructed from the raw data.

The software used for this task is called *MultiFit*. It has been developed by Matthias Enno Janssen⁹ and makes use of the LCIO[11] and ROOT[12] software frameworks.

MultiFit is divided into three main steps. The operation of the steps is independent of each other but the results from the previous step are required as input of the next one.

1. In the first step connected charge depositions are detected row by row and combined to three dimensional track points called *hits*. This procedure is called *cluster finding*.
2. Next hits belonging to one particle track are grouped together, which is called *track finding*.
3. The last step is the *track fitting*. Here a function is fitted to the hits belonging to one track. This fit function offers geometrical properties of the track.¹⁰

After this last step the reconstruction is completed and real physical analysis of the track data – or the analysis of the performance of the MultiFit algorithms – can start.

MultiFit is controlled via plain text configuration files. Each step offers several parameters which can be adjusted.¹¹ MultiFit can use LCIO or ROOT files for input. The output, the pulse, hit and track information, is saved as a ROOT tree.

In the following sections the reconstruction with MultiFit is explained in more detail. The coverage is not complete and only the steps relevant for this work are depicted in detail. More information can be found in the theses cited above.

Before starting with the discussion, a coordinate system is introduced. The x direction is a horizontal and the y direction is a vertical axis along the pad plane. The z axis points into the gas volume of the TPC. The origin of this system is the

⁹The work is documented the theses [6],[7] and [8].

¹⁰e.g. the angle ϕ of the track in the xy plane

¹¹e.g. the layout of the pad plane and the mapping of the TPD channels to the logical pad plane layout have to be specified

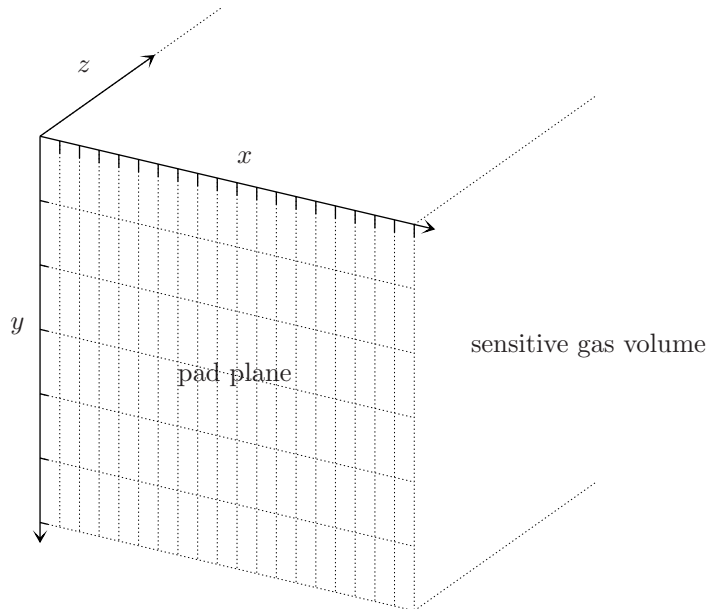


Figure 4: Coordinate system used in MultiFit

upper left corner of the pad plane – viewed from outside the TPC (compare Fig. 4).

3.2.1 Cluster Finding

In the first step the time information has to be transformed in a z position. This is established using $z = v_D t$, where t is the time since the passage of the muon which triggered the event. The drift velocity can be computed theoretically or extracted from the measurements, which will be discussed later.

After this transformation the whole event is represented by a set of small three dimensional volume elements (voxels) and a charge deposition is assigned to each voxel.

In the next step *pulses* are formed. A pulse is the charge deposition on a single pad (in the xy plane) belonging to one track. To determine a pulse for each pad the corresponding voxels in z direction have to be regarded (compare Fig. 5).

Voxels with charge depositions under a certain threshold are discarded and the remaining connected voxels are combined to pulses. The charge of a pulse is, apart from a minor correction, the sum of the charge depositions of the voxels. For each pulse a z position is calculated from the z positions of the associated voxels.

In the next step adjacent pulses in one row are connected to *hits*. In order to avoid false allocations, the z position of the pulses are taken in account during this process. So only pulses adjacent in x direction within a certain limited distance in z direction (called *search window*) are combined to a hit (compare Fig. 6).

Finally the coordinates of the hit are computed. The y coordinate is the middle

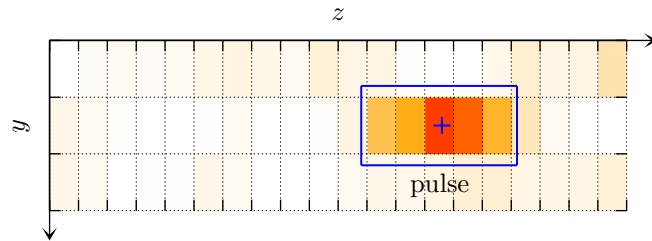


Figure 5: Voxels in z direction belonging to pads at positions (x, y) on the pad plane shown in yz projection

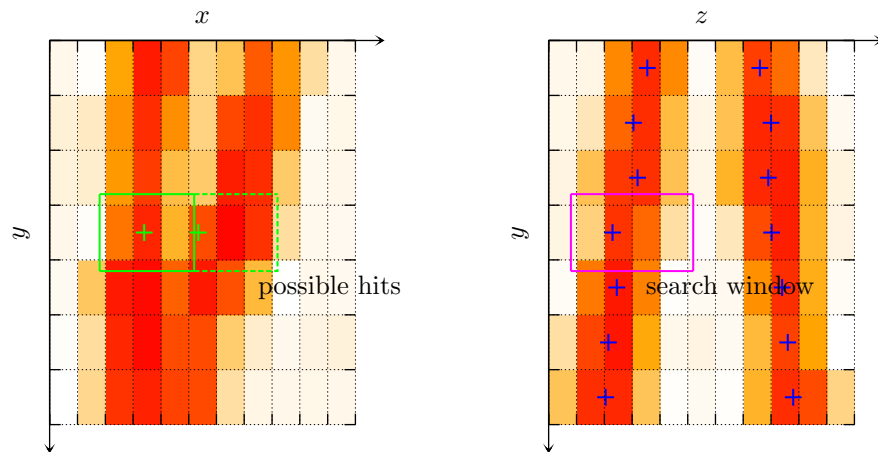


Figure 6: The xy projection is not sufficient to decide which pulses belong to one hit. The search window in the yz projection is needed.

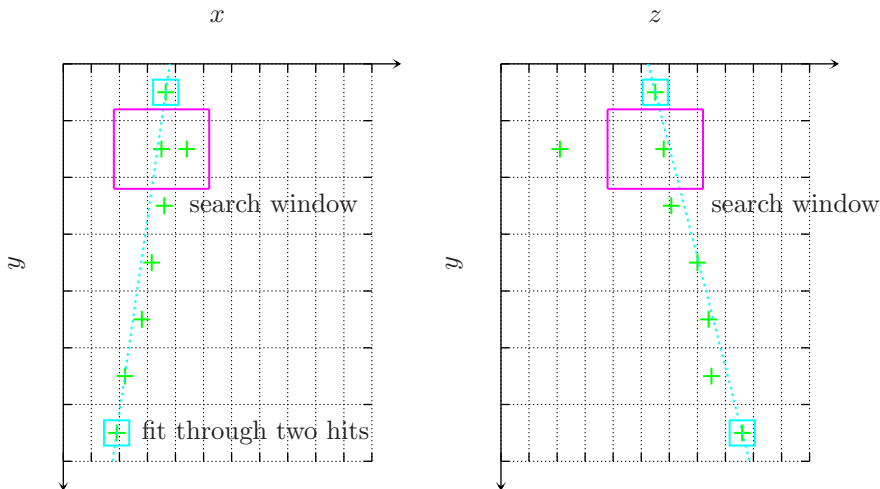


Figure 7: To avoid ambiguities, the track finding algorithms have to be restricted using a search window in the z direction.

of the row. To determine the x position, a center of gravity method is employed¹²:

$$x_{\text{hit}} = \frac{\sum_{\text{pulses}} Q_{\text{pulse}} x_{\text{pulse}}}{\sum_{\text{pulses}} Q_{\text{pulse}}}$$

The remaining z position of the hit is also calculated using the center of gravity approach.

3.2.2 Track Finding

After the construction of the hits, the hits are combined to *tracks*.

A relatively simple algorithm is used which only works well for particle tracks with a rather small curvature, which means high energetic particles.

First two hits with a certain distance on the pad plane are chosen and a straight line is fitted through them. Starting from the upper of both hits a third hit is searched one row below. This hit has to lie in defined search windows around the fitted line in the xy as well as the yz projection (compare Fig. 7).

If a third hit is found, a straight line is fitted through all three hits and the fourth hit is searched using the same algorithm. This procedure is continued through all rows.

All hits found are then grouped into one track collection.

3.2.3 Track Fitting

In order to fit a geometrical function to the hits of a track, different algorithms are implemented in MultiFit. In this work only a brief introduction is given.

3.2.3.1 GlobalFit The *GlobalFit* algorithm is a numerical likelihood¹³ fit of a gaussian charge distribution with constant width of a circular track in the xy and a straight track in the yz projection to the pulses.

There are two variations of this algorithm implemented. If the width of the charge distribution is fixed¹⁴ before the fit, we name the algorithm GlobalFit with

¹²Here Q_{pulse} denotes the charge of the pulse.

¹³An introduction to likelihood maximization can be found in [9].

¹⁴by $\sqrt{D^2z + \sigma_0^2}$, where D and σ_0 the constants given in Tab. 1

fixed σ . The case that the width is a parameter of the fit, the algorithm is called GlobalFit with *free* σ .

A speciality of GlobalFit is that it does not use the hits and the results of the track finding. Instead it is based directly on the pulses.

3.2.3.2 χ^2 Fit This algorithm employs a χ^2 minimization¹⁵ of a circular arc in the xy projection and of a straight line in the yz projection. These functions are fitted to the hit positions.

To get reasonable initial values for the fit of the arc a polynomial function of the form

$$x = f(y) = ay^2 + by + c$$

is fitted to the hit positions first. Then $R = a/2$ is an approximation for the radius R of the circular arc. Furthermore the center of the circle (x_0, y_0) is estimated by solving the equation

$$(x - x_0)^2 + (y - y_0)^2 = R^2$$

for two points $(f(y), y)$ on the graph of the polynomial.

Finally the arc is described by the function

$$x = f(y) = x_0 \pm \sqrt{R^2 - (y - y_0)^2}$$

is fitted to the hit positions using the initial values of x_0 , y_0 and R from the previous step.

3.2.4 Pad Response Correction

3.2.4.1 Incorrect Hit Reconstruction As mentioned above, the x position of a hit is calculated using a center of gravity method for the single pulses. This computation offers correct results for charge signals with a large signal width¹⁶ σ_{signal} . In this case the charge is deposited on many¹⁷ pads. Under these circumstances we can assume¹⁸:

$$x_{\text{hit}} \approx \langle x \rangle =: x_{\text{signal}}$$

For small signal widths this approximation does not hold. If a signal strikes mainly one pad and there is only little charge deposition on other pads, then the reconstructed hit position x_{hit} is shifted towards the center of the pad with major charge deposition. This is illustrated in Fig. 8. In this figure and in the rest of this section all metric units are normalized to the pad width¹⁹ and the origin of the x axis is chosen to be the center of a pad with the highest signal.

For a signal width $\sigma_{\text{signal}} = 0.18$ the dependence of x_{hit} and x_{signal} is shown in Fig. 9. The curve in this figure is obtained from a simulation. The deviation of the curve $x_{\text{hit}}(x_{\text{signal}})$ from identity shows the same effect as described using the example of a narrow signal above. Signals get reconstructed towards the center of the pad.

As a result of the incorrect hit reconstruction the point resolution is affected in a negative way.

¹⁵The χ^2 fit is also described in [9].

¹⁶We assume the charge distribution to be gaussian. The width is then the width of the Gaussian.

¹⁷4 or more

¹⁸ $\langle x \rangle$ is the mean value of the true charge distribution of the signal.

¹⁹For convenience we omit writing this special normalization explicitly. We also omit the unit of charges in this section.

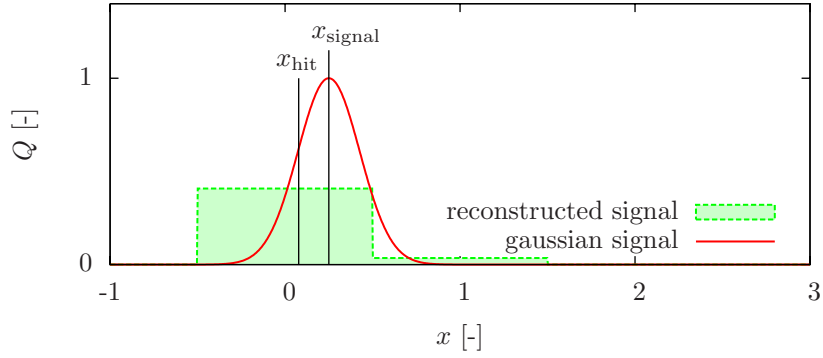


Figure 8: Narrow signal with main charge deposition on a single pad. Reconstructed hit position x_{hit} and true signal position x_{signal} do not agree.

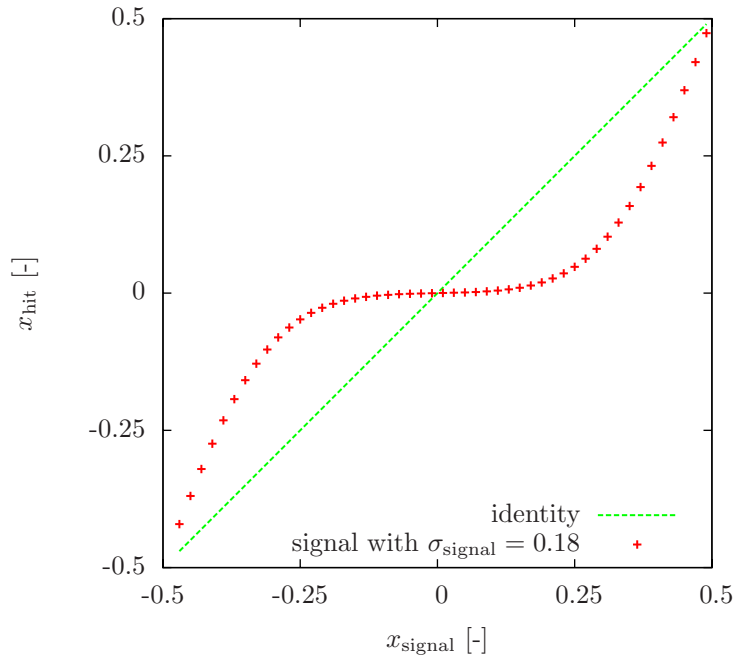


Figure 9: Dependency of the hit position x_{hit} on the signal position x_{hit} for a signal of width $\sigma_{\text{signal}} = 0.18$.

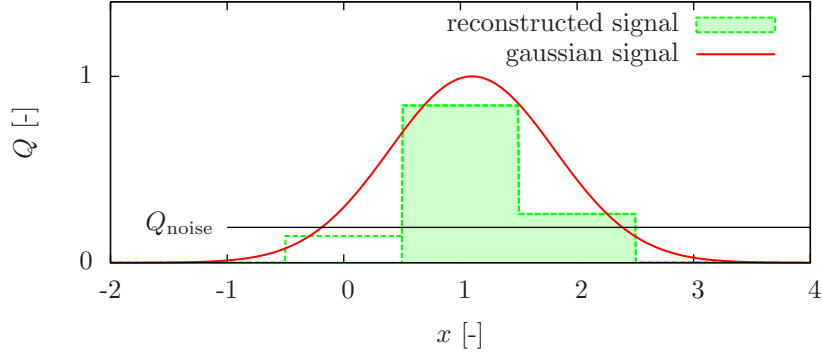


Figure 10: Pad response signals below a the threshold Q_{noise} are not included in the calculation of x_{hit} .

3.2.4.2 Correction of Hit Position In MultiFit an algorithm called *Pad Response Correction* (PRC) is implemented which tries to correct the hit positions x_{hit} to overcome the above issues. The basic idea of this algorithm is to find a functional relation between the wrongly reconstructed hit position x_{hit} and the true signal position x_{signal} depending on the signal width σ_{signal} (see Fig. 9). If such a function is known, the hit positions can be corrected. The corrected hit positions are called x'_{hit} .

To realize this idea, a row of a few pads of width $p = 1$ that are hit by gaussian signals of height $Q_{\text{signal}} = 1$ and fixed width σ_{signal} is simulated. The charge deposition on each pad results from the *Pad Response Function* (PRF)[2]:

$$Q_{\text{pad}}(x_{\text{signal}}) = \int_{-p/2}^{p/2} \frac{Q_{\text{signal}}}{\sqrt{2\pi}\sigma_{\text{signal}}} \exp\left(-\frac{(x - x_{\text{signal}})^2}{2\sigma_{\text{signal}}^2}\right) dx$$

The signals from these pads are then interpreted as pulses of a hit and the hit position x_{hit} is calculated according to the center of gravity method.

There is one further aspect which has to be taken in account. Due to noise a threshold was introduced during the pulse reconstruction (compare Sec. 3.2.1). Such a threshold Q_{noise} is also used in the simulation. Consequently if $Q_{\text{pad}}(x_{\text{signal}}) < Q_{\text{noise}}$, we set $Q_{\text{pad}}(x_{\text{signal}}) = 0$ (compare Fig. 10). In the simulation a threshold of $Q_{\text{noise}} = 0.001$ is used.

In case this threshold causes a signal to be counted merely on one pad, which is the case for small signal widths, information is lost because then the signal is always reconstructed to the center of the pad.

The resulting data points $x_{\text{signal}}(x_{\text{hit}})$ are shown in Fig. 11 for different signal widths σ_{signal} . For small values of σ_{signal} , due to the threshold, the function $x_{\text{signal}}(x_{\text{hit}})$ is not continuous at $x_{\text{hit}} = 0$. This implies that for signal positions x_{signal} in a certain interval around 0 we get $x_{\text{hit}} = 0$, which means that in this case the hit position cannot be corrected.

Due to the symmetry of Fig. 11, to implement the PRC in MultiFit functions are fitted to the data points for each signal width only for $x_{\text{hit}} > 0$ σ_{signal} :

$$f_{\text{not flat}}(x_{\text{hit}}, \sigma_{\text{signal}}) = b_1 x_{\text{hit}} + b_2 \sqrt{x_{\text{hit}}} + \left(\frac{1 - b_1}{2} - \frac{b_2}{\sqrt{2}}\right) \sqrt[3]{2x_{\text{hit}}}$$

$$f_{\text{flat}}(x_{\text{hit}}, \sigma_{\text{signal}}) = c_0 + c_2 \sqrt{x_{\text{hit}}} + \left(\frac{1 - 2c_0}{2} - \frac{c_2}{\sqrt{2}}\right) \sqrt[3]{2x_{\text{hit}}}$$

The coefficients $b_i = b_i(\sigma_{\text{signal}})$ and $c_i = c_i(\sigma_{\text{signal}})$ are of course functions of σ_{signal} ,

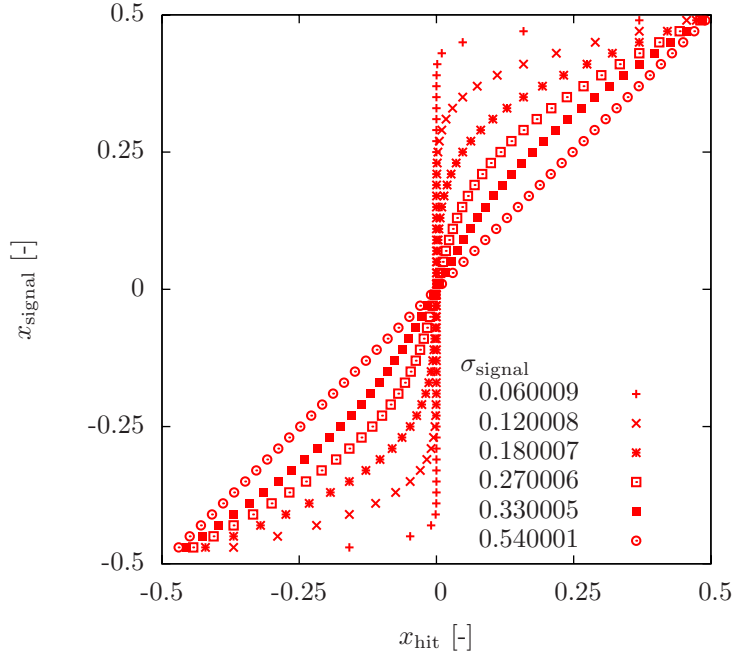


Figure 11: Dependency of the hit position x_{hit} on the signal position x_{hit} for different signal widths σ_{signal} .

b_1	a_{15} [-]	a_{14} [-]	a_{13} [-]	a_{12} [-]	a_{11} [-]	a_{10} [-]
	-832.583	1936.17	-1739.82	739.665	-141.994	9.52257
b_2	a_{25} [-]	a_{24} [-]	a_{23} [-]	a_{22} [-]	a_{21} [-]	a_{20} [-]
	1398.15	-3350.91	3126.27	-1399.78	292.479	-21.2726
c_0	a_{01} [-]	a_{00} [-]				
	0.49900	0.12800				
c_2	a_{26} [-]					
	-4.21678					

Table 2: Coefficients for the PRC algorithm

too. The fitted coefficients b_i and c_i as well as the χ^2 of the fit are shown as functions of σ_{signal} in Fig. 12.

The χ^2 value of the fit is used to decide whether to use f_{flat} or $f_{\text{no flat}}$ for the correction of the hit position. The function with the smaller χ^2 is used, which turns out to be f_{flat} for $\sigma_{\text{signal}} < 0.128 =: \sigma_{\text{boundary}}$ and $f_{\text{not flat}}$ for $\sigma_{\text{signal}} \geq \sigma_{\text{boundary}}$.

In the next step the parameters b_i and c_i in Fig. 12 are fitted using the functions²⁰:

$$\begin{aligned}
 b_1(\sigma) &= a_{15}\sigma^5 + a_{14}\sigma^4 + a_{13}\sigma^3 + a_{12}\sigma^2 + a_{11}\sigma + a_{10} \\
 b_2(\sigma) &= a_{25}\sigma^5 + a_{24}\sigma^4 + a_{23}\sigma^3 + a_{22}\sigma^2 + a_{21}\sigma + a_{20} \\
 c_0(\sigma) &= a_{01}(1 - \sigma)/a_{00} \\
 c_2(\sigma) &= a_{26}\sigma
 \end{aligned}$$

The values obtained by the simulation are shown in Tab. 2.

During the reconstruction of real data the true signal width of the hits is not known. For the PRC the signal width is approximated using a equation similar

²⁰For simplicity the subscript of σ_{signal} in these equations has been dropped.

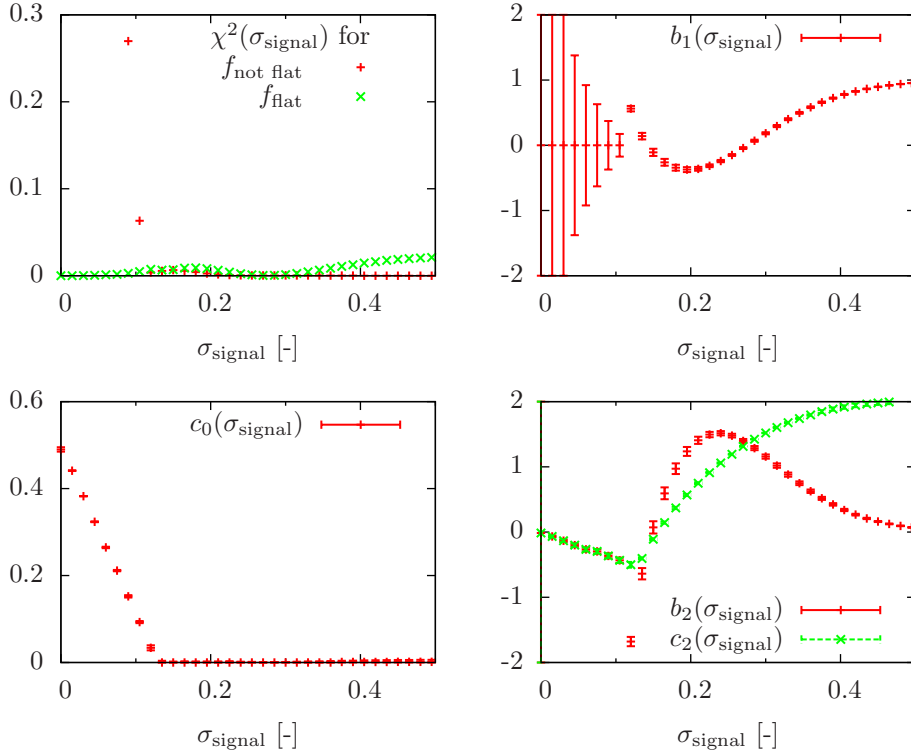


Figure 12: Fitted coefficients b_i and c_i as well as the χ^2 as functions of σ_{signal}

to Eq. 4: $\sigma_{\text{signal}} = \sqrt{D^2 z + \sigma_0^2}$. Therefore the diffusion coefficient D and the defocusing constant σ_0 have to be specified in the MultiFit configuration file.

The corrected hit positions are finally defined as²¹:

$$x'_{\text{hit}}(x_{\text{hit}}) = \text{sgn}(x_{\text{hit}}) \begin{cases} f_{\text{flat}}(x_{\text{hit}}, \sigma_{\text{signal}}) & \text{if } \sigma_{\text{signal}} < \sigma_{\text{boundary}} \\ f_{\text{not flat}}(x_{\text{hit}}, \sigma_{\text{signal}}) & \text{if } \sigma_{\text{signal}} \geq \sigma_{\text{boundary}} \end{cases}$$

In the reconstruction the PRC is applied to correct the hit positions before using the χ^2 track fitting algorithm. To distinguish these results from track fits with uncorrected hit positions we introduce the notation: χ^2 fit *with PRC* and χ^2 fit *without PRC*.

3.3 ROOT Analysis Scripts

After the tracks are reconstructed using MultiFit the analysis which is based on these tracks can start. Since the output of MultiFit is a ROOT tree, ROOT script are used to analyze the data.

For many standard tasks there are already scripts available. Here only the concepts on which two frequently used scripts are based are described.

3.3.1 Point Resolution

One important task is to calculate the transverse point resolution.

Theoretically the hits are distributed in a gaussian way around the true track. The width of this distribution is a measure for the resolution.

²¹Here $\text{sgn}(x)$ denotes the signum function which is 1 for an argument $x \geq 0$ and -1 for $x < 0$.

Unfortunately the true track is not known, but only the position of the fitted track. To use this data for determining the resolution we introduce two quantities. The *distance* d of a hit is the difference of the x position of the fitted track x_{fit} and the x position of the hit x_{hit} . Which means: $d = x_{\text{fit}}(y_{\text{hit}}) - x_{\text{hit}}$. The *residual* r denotes the difference between the x position of a fitted track where the current hit has not been taken into account for the fit, $x_{\text{fit, without hit}}$, and x_{hit} – as a formula: $r = x_{\text{fit, without hit}}(y_{\text{hit}}) - x_{\text{hit}}$. The orthogonal distance respectively residual are then defined as:

$$\begin{aligned} d' &= d \cos \phi_{\text{hit}} = (x_{\text{fit}}(y_{\text{hit}}) - x_{\text{hit}}) \cos \phi_{\text{hit}} \\ r' &= r \cos \phi_{\text{hit}} = (x_{\text{fit, without hit}}(y_{\text{hit}}) - x_{\text{hit}}) \cos \phi_{\text{hit}} \end{aligned}$$

Here ϕ_{hit} is the angle of between the y axis and the track at the position of the hit $y = y_{\text{hit}}$. It can be derived from the track angle ϕ and the radius R :

$$\phi_{\text{hit}} = \arcsin \left(\sin \phi - \frac{y_{\text{hit}}}{R} \right)$$

In this case ϕ is the angle between the y axis and the track at $y = 0$.

Using these definitions it can be shown that, at least for straight tracks, the transverse point resolution is given by the geometric mean is the width of both distributions[10]:

$$\sigma_T = \sqrt{\sigma_{d'} \sigma_{r'}}$$

Furthermore the script for resolution analysis offers the possibility to cut the data on predefined hit angles ϕ_{hit} , which means that only hits with a hit angle in a certain range are taken into account.

3.3.2 Drift Velocity

To determine the drift velocity the cluster finding step of MultiFit is started with an approximate drift velocity.

Using the output of this step a histogram of the drift times t is created. This histogram drops abruptly to 0 for a time called t_L . We interpret this as the time a electron from cathode needs to drift through the whole chamber to reach the readout at the anode. Since the length L of the chamber is known, the drift velocity v_D can be calculated to be:

$$v_D = \frac{L}{t_L}$$

Identifier	B [T]	Pad pitch [mm ²]	Pad layout	No. of events
0045	1	1.27×6.985	non-staggered	87725
0052	3	1.27×6.985	non-staggered	36591

Table 3: Settings of measurement runs

4 Analysis and Results

The analysis is carried out for data measured with the *small* 1.27×6.985 mm² pads. Sometimes the results are compared with measurements using *large* 2.2×6.2 mm² pads.

4.1 Track Reconstruction

The first step of the data analysis is the reconstruction of the particle tracks using MultiFit. This step is done for the runs shown in Tab. 3. Before a complete MultiFit run including track fitting can be started, some preparatory steps are necessary.

4.1.1 Preparing the Reconstruction

4.1.1.1 Defect Pads and Different Thresholds For searching damaged pads only the output of the MultiFit cluster finding procedure is needed.

A ROOT script offers a graphical overview of the charge accumulation during the whole event on each pad on the pad plane. Using this plot defect channels and pads with exceptionally high or low intensity are identified manually and disabled in the MultiFit configuration file. A charge deposition plot of the whole pad plane is shown in Fig. 13.

Furthermore a histogram of the charge deposition and a plot of the average pulse shape is created for each pad by the same script. These plots are also used to identify defect channels.

This procedure is carried out for different threshold settings. Low thresholds cause much noise and many pads showing an abnormal behavior. On the other hand an as low as possible threshold is preferred to allow an accurate charge measurement.

In the end a threshold with as few defects pads as possible is chosen.

4.1.1.2 Problem with Readout Electronics Some measurement runs show a very unusual charge distribution on the pad plane after a certain number of events. A large number of pads shows only a very low charge deposition. These events are excluded from further analysis.

It turned out that the data from these pads was digitized by the same TPD. A closer investigation showed that the connection between the trigger and the TPD was defect. This has been repaired in the meantime.

4.1.1.3 Drift Velocity Next the drift velocity for the current measurement run is determined using the method depicted in Sec. 3.3.2.

4.1.2 Track Fitting

After these preparations a full MultiFit run including cluster finding, track finding and track fitting is started. For each measurement run four different fitting algorithms are used: χ^2 fit with PRC, χ^2 without PRC, GlobalFit free σ and GlobalFit fixed σ .

For the χ^2 fit with PRC and GlobalFit with fixed σ the appropriate diffusion coefficient and defocusing constant, listed in Tab. 1, are used.

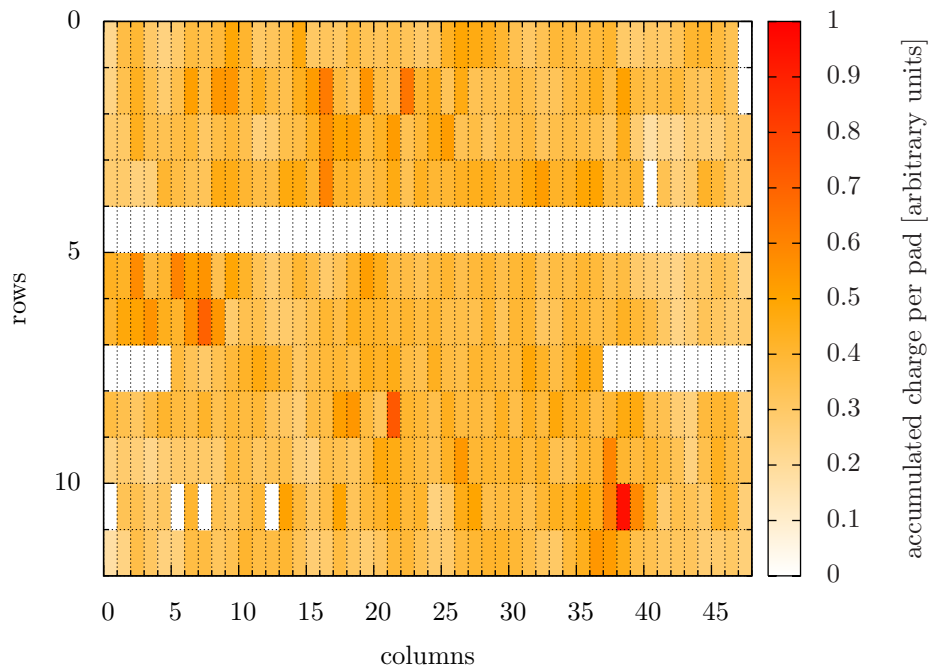


Figure 13: Charge accumulation on the pad plane for the 3T run and a threshold of 10; the white pads are defect or not connected

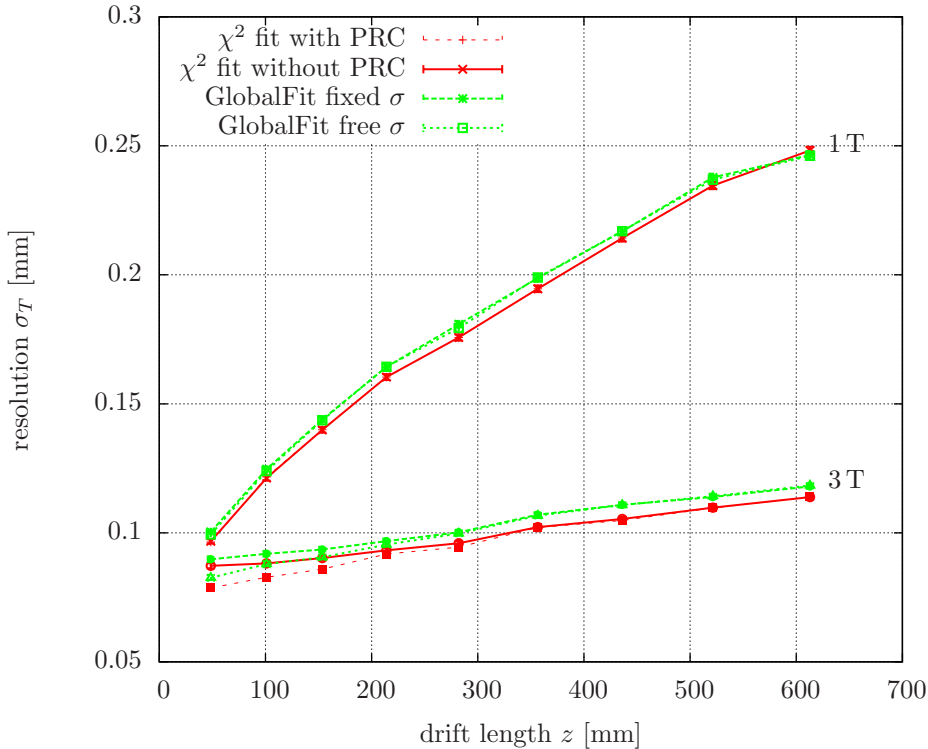


Figure 14: Resolution with small pads for different magnetic fields

4.2 Point Resolution

A cut on the hit angle ϕ_{hit} is used for all resolution calculations. Only hits with $|\phi_{\text{hit}}| < 0.1$ rad are included in the results. This limit was agreed upon inside an international collaboration to make resolution results from different groups comparable.

4.2.1 Comparison between Small and Large Pads

In Fig. 14 the transverse point resolution²² is plotted as a function of the z coordinate respectively the drift length for different fitting algorithms and magnetic fields.

One obvious effect is the increase of the resolution for large drift distances z . This observation agrees qualitatively with the lower bound of the resolution given by Eq. 4, which also increases with z . The increase of the resolution is suppressed drastically for the high magnetic fields – in this case a 3 T field. At least the qualitative aspect of this behavior can also be understood theoretically as mentioned in Sec. 2.1.2 and furthermore manifests in the diffusion constants in Tab. 1.²³

There is hardly a difference between the four fit algorithms, although the χ^2 fit systematically offers a better resolution than the GlobalFit algorithm. Especially the two variants of each algorithm²⁴ cannot be distinguished. There is one exception regarding the 3 T run for small drift length z . In this case there is a difference and the resolution is improved by the PRC.

²²from now on referred to just as *resolution*

²³although these constants are not directly the constants D' and σ'_0 in Eq. 4

²⁴with PRC and without PRC for the χ^2 fit and free σ resp. fixed σ for GlobalFit

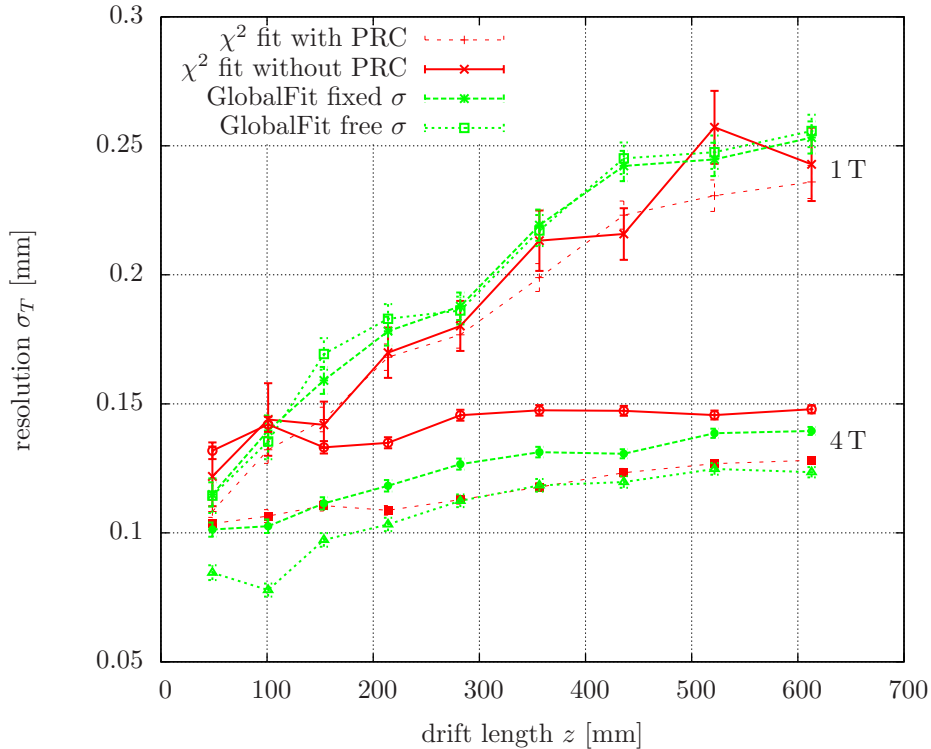


Figure 15: Resolution with large pads for different magnetic fields

In Fig. 15 the resolution for large pads is plotted for different magnetic fields. One important aspect is that in this case there is a difference between the different variants of the fitting algorithms.

The resolution results for small and large pads with PRC are compared in Fig. 16.

First this comparison shows that for a magnetic field of 1 T there is only a little difference in the resolution. For higher fields the situation changes. Although a 3 T run with small pads is compared with a 4 T run with large pads, the resolution with the small pads is clearly better and stays below 0.1 mm up to a drift length of about 350 mm. The resolution of the run with large pads stays above this limit for all distances.

A resolution of 0.1 mm over the whole length of the chamber is a upper limit for TPC prototypes because such a resolution enables the realization of physics goals at a future ILC detector. A measurement with a magnetic field of 4 T would fulfill this aim for an even larger range of drift lengths.

4.2.2 Angular Dependency

Next the angular dependency of the resolution has been analyzed. Here only the measurement run with the small pads and a magnetic field of 3 T is used. In Fig. 17 and Fig. 18 the dependency of the resolution on the hit angle ϕ_{hit} is shown.

One important aspect to notice is that the resolution of all algorithms gets worse for larger angles. For the χ^2 fit this can be explained by the way the hit finding works. There worst case is a horizontal track²⁵. Because pulses are combined line by line, in this case all pulses are combined to only one hit with an extremely large

²⁵track angle $\phi = \pi/2$

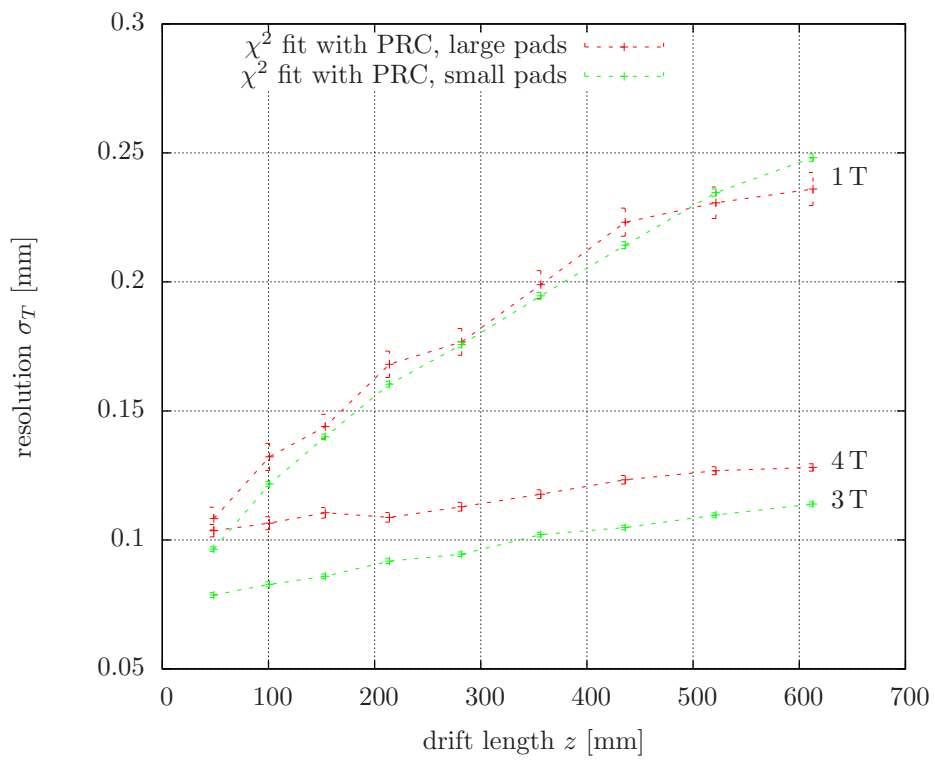


Figure 16: Comparison of the resolution with large and small pads for the χ^2 fit with PRC

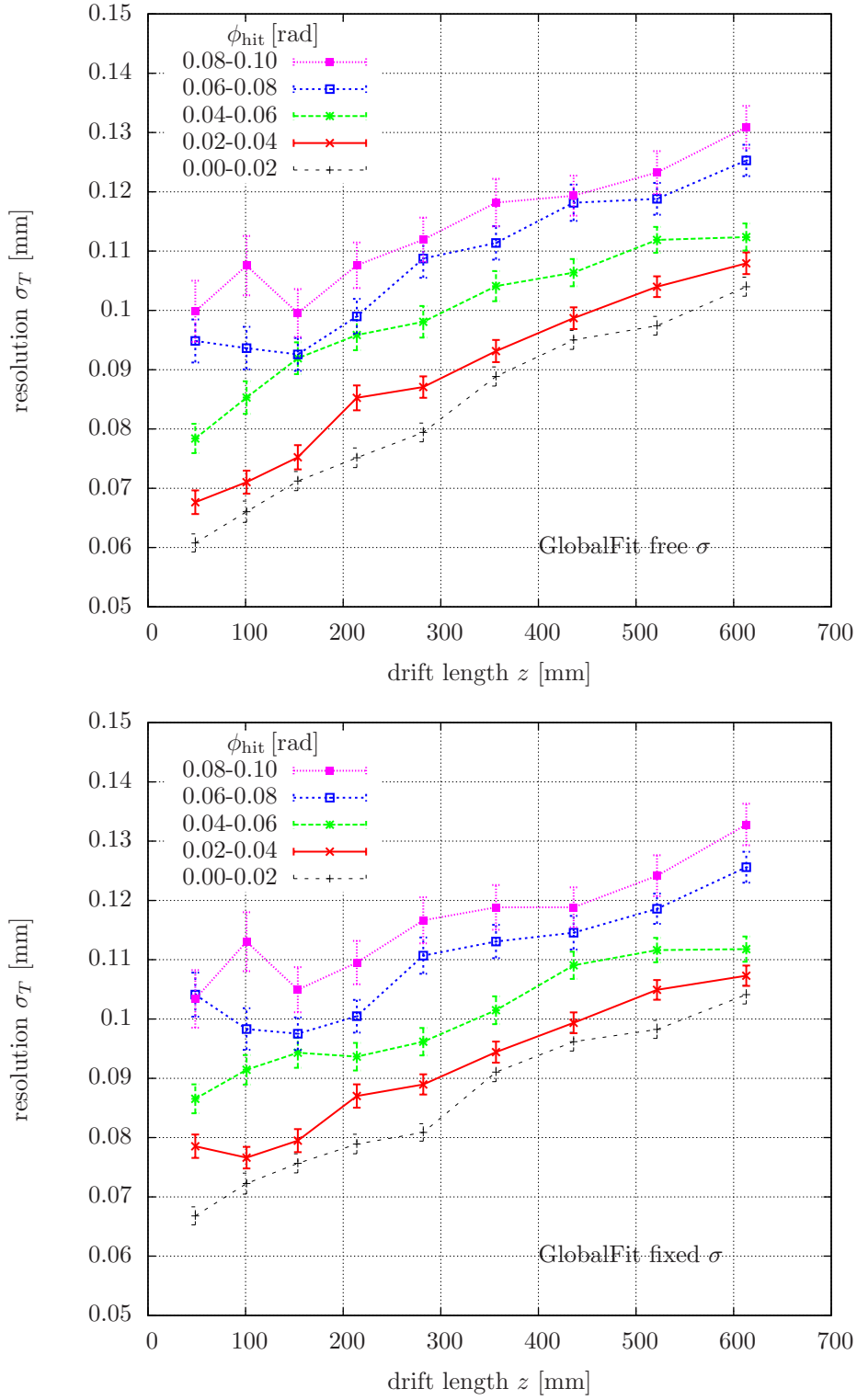


Figure 17: Resolution for different cuts on the hit angle ϕ_{hit} using GlobalFit with free σ (upper plot) and fixed σ (lower plot)

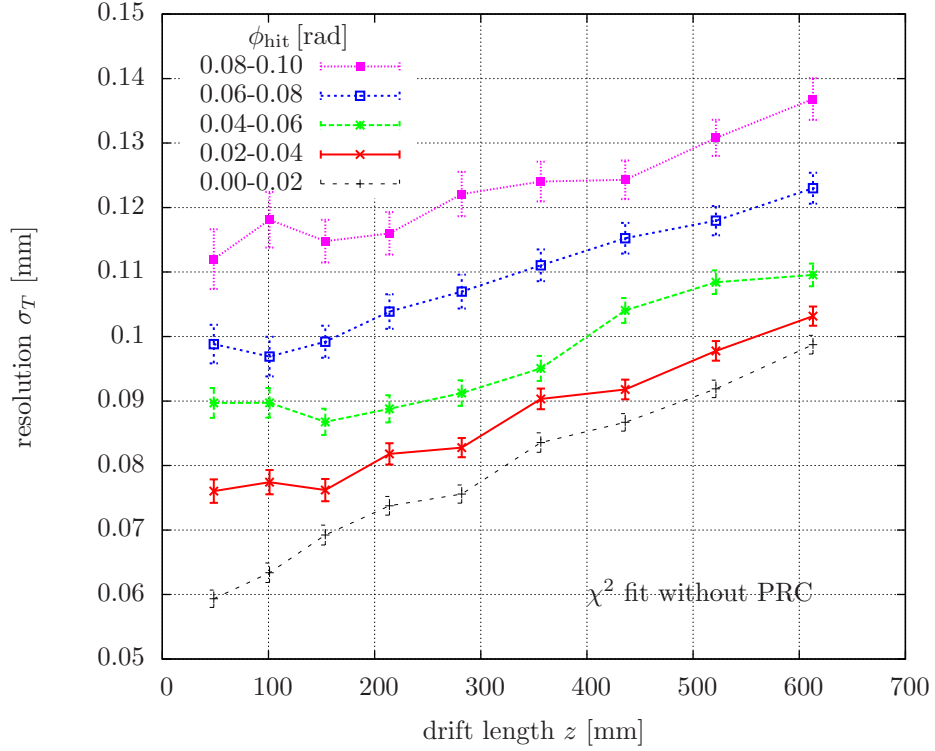
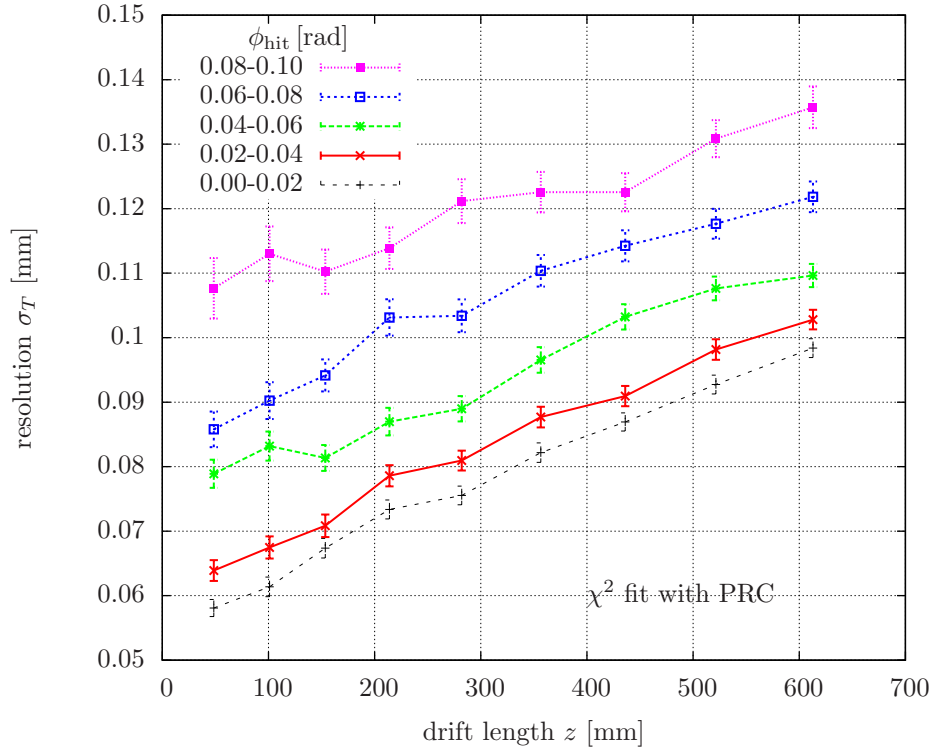


Figure 18: Resolution for different cuts on the hit angle ϕ_{hit} using the χ^2 fit with PRC (upper plot) and without PRC (lower plot)

width. This makes a meaningful track fitting impossible and causes large errors. Also because of the line-by-line method vertical tracks²⁶ can be constructed most precisely. The observed angular dependency of the resolution can be understood by interpolating between both cases.²⁷

Comparing Fig. 17 and Fig. 18 the decline of the resolution with an increasing hit angle is more distinctive with the χ^2 fits. The relatively good performance of the GlobalFit can be explained by a handling of angular tracks already included in the GlobalFit algorithm[6].

Right now the PRC algorithm cannot handle angular tracks correctly. And one possible extension of the algorithms is to implement handling of angular tracks. However, as also visible on Fig. 18, for drift lengths up to 200 mm the PRC improves the resolution regardless of the angle cut.

²⁶track angle $\phi = 0$

²⁷A more quantitative description of angular effects can be found in [10].

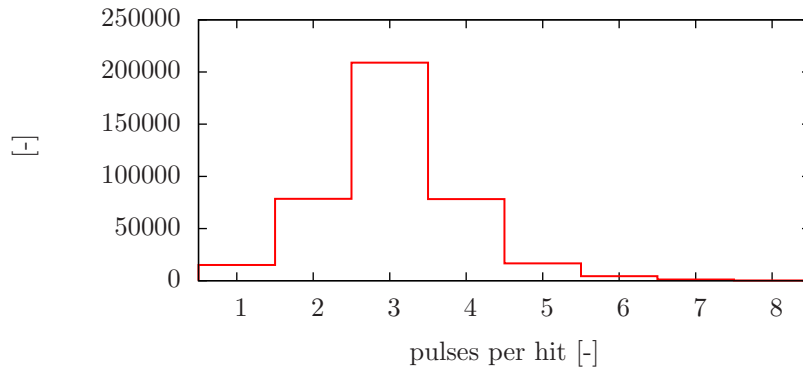


Figure 19: Histogram of the pulses per hit

4.3 Pad Response Correction

4.3.1 Pad Response

To get a first impression of the effect of the pad geometry on the charge distribution a histogram of the positions of the hits x_{hit} is shown in Fig. 20 for different binnings.²⁸

Using the binning the distribution looks flat for the relevant range of x positions. With more bins sharp peaks become visible. These peaks are exactly in the middle of the pads and are caused by hits that consist of only one pulse.

It is important to notice that the effects of hits with a width of only one pad cannot be corrected by the PRC (compare Fig. 11) since these hits are reconstructed to the center of a pad.

Fig. 19 shows a histogram of the number of pads belonging to a hit. By the number of hits with only one pulse we can estimate that the PRC has no effect for at least 4% of the hits.

²⁸We use data of the 3 T run with small pads in this section.

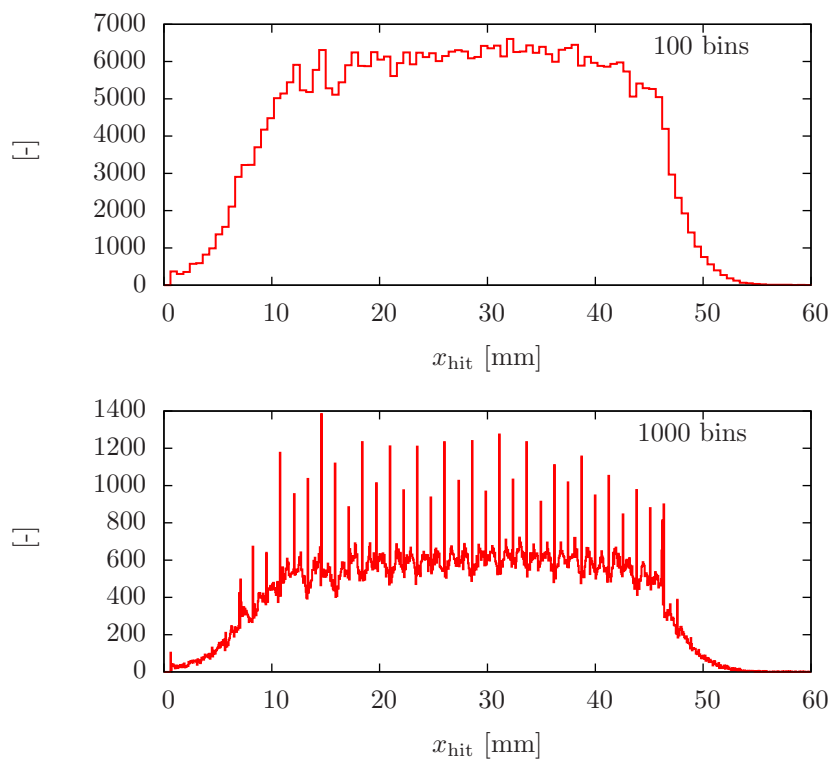


Figure 20: Histogram of the hit positions x_{hits} for 100 bins (upper plot) and 1000 bins (lower plot)

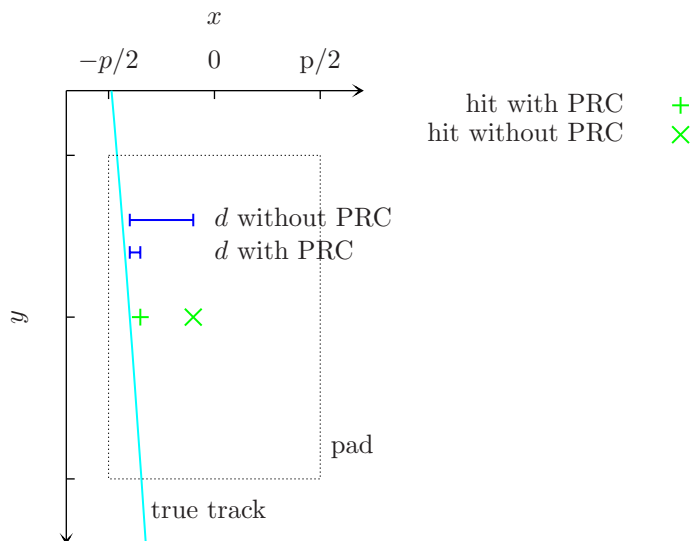


Figure 21: Track traversing the left side of a pad with reconstructed (without PRC) and corrected (with PRC) hit position

4.3.2 Quality of the Pad Response Correction

4.3.2.1 Introduction to the Method To get, apart from the resolution (Sec. 4.2), another measure for quality of the PRC we analyze a two-dimensional histogram of all hits with the position where the track traverses the pad²⁹ x_{track} modulo the pad width p on the one axis and the distance of the hit d on the other axis. The modulo operation has the effect that the hits on all pads are overlaid.

If we neglect the influence of the pad geometry, we do not expect a dependency of the distance (compare Sec. 3.3.1) on the track position.

In reality we have to distinguish between the results with and without PRC.

First we discuss the expectations for the hits calculated without PRC. If the track traverses the pad on the left side of the pad³⁰, the hit is reconstructed erroneously in the direction of the center of the pad (compare Fig. 11 and Fig. 21). This causes the absolute value of the distance of this hit to be larger than the absolute value of the distance of the true signal. If we include the signs in the definition of the distance (compare Sec. 3.3.1), we get a negative distance. Therefore in the two-dimensional histogram for $x_{\text{track}} < p/2$ we expect many entries with a distance $d < 0$. The same argument holds for a track traversing the right side of a pad ($x_{\text{track}} > p/2$). In this case we conclude that there have to be many entries with a distance $d > 0$.

For hit positions computed with the PRC algorithm we expect a histogram looking more like the ideal case without influence of the pad geometry.

There is one difficulty using this approach. Since we are analyzing measured data and have no external reference like for example Monte Carlo studies, the true track position is not known. Hence we use the tracks of the χ^2 fit with PRC as reference. And the hit distances d for the hit positions with and without PRC are computed with respect to these tracks.

Furthermore we await artifacts due to those hits with only one pulse because their reconstructed position is always the center of the pad. Therefore in the fol-

²⁹called track position from now on

³⁰which means $x_{\text{track}} < p/2$

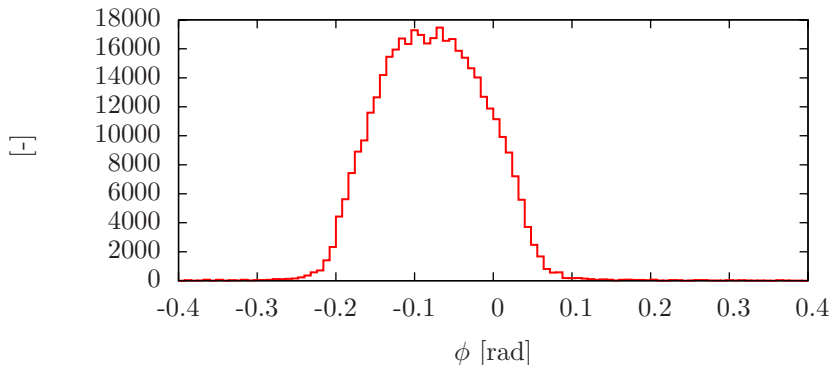


Figure 22: Distribution of the track angle ϕ

lowing analysis only hits consisting of more than one pulse are regarded.

4.3.2.2 Small Pads The results for the pad plane with small pads and a magnetic field of 3 T are shown in Fig. 23.

On the two-dimensional histogram of the results without PRC the expected shape can hardly be seen. So for each value of x_{track} a mean value of all distances is calculated. The results are shown in Fig. 23 at the bottom.

In this plot the expected behavior is visible at least for the hits without PRC. Unfortunately the curve with PRC also has a sinusoidal shape with nearly the same amplitude, but a different sign. The PRC seems to overcompensate the wrong hit positions.

Another aspect of the diagram of the mean values is the mirror symmetry regarding the line given by a distance of about $d = 0.02 \text{ mm}$. In contrast to this observation we would expect a symmetry regarding the $d = 0 \text{ mm}$ axis since the distance should be distributed symmetrically.

4.3.2.2.1 Angle Cut The same data as above is also analyzed with a cut on the track angle ϕ . The results in Fig. 24 include only hits from tracks with $|\phi| < 0.02 \text{ rad}$.

In the plot of the mean value the amplitude of the curve of the results with PRC is much smaller than without the angle cut. The amplitude decreased from about 0.01 mm to about 0.005 mm . This plot agrees much more with the expectations for the effect of the PRC.

In this case a clear dependence of the quality of the PRC algorithm on the angle can be seen. This indicates that including an angular dependency in the PRC might have positive effects.

Furthermore we recognize that in Fig. 24 the offset of the symmetry axis disappeared. This suggests that the offset in Fig. 23 is caused by an asymmetric angle distribution of the track angle ϕ (compare Fig. 22) which has no effect in case of the angle cut.

4.3.2.3 Large Pads For comparison the above method is also used to analyze data from a run with large pads and a magnetic field of 4 T (see Fig. 25).

First the few entries in the middle of the pad are peculiar. However this phenomenon can be explained because of the large pad size there are many hits with only one pulse, which are still excluded from the plots. All these hits are reconstructed to the center of the pad and due to the cut there are fewer hits in the region around the center.

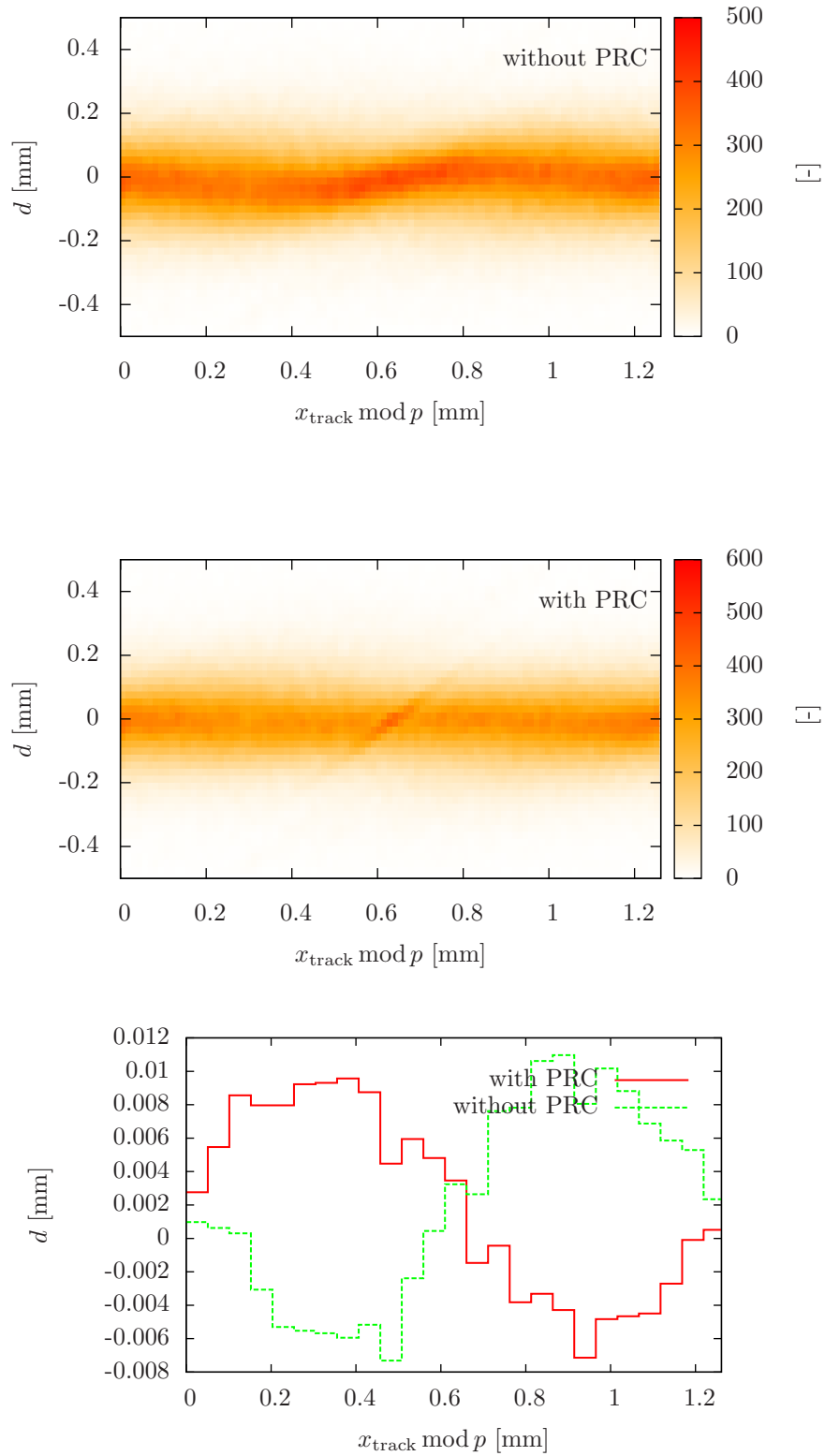


Figure 23: PRC quality plot for small pads; two dimensional histogram of track position $x_{\text{track mod } p}$ and distance d for hits computed without and with PRC, plot of the mean distances from the upper diagrams

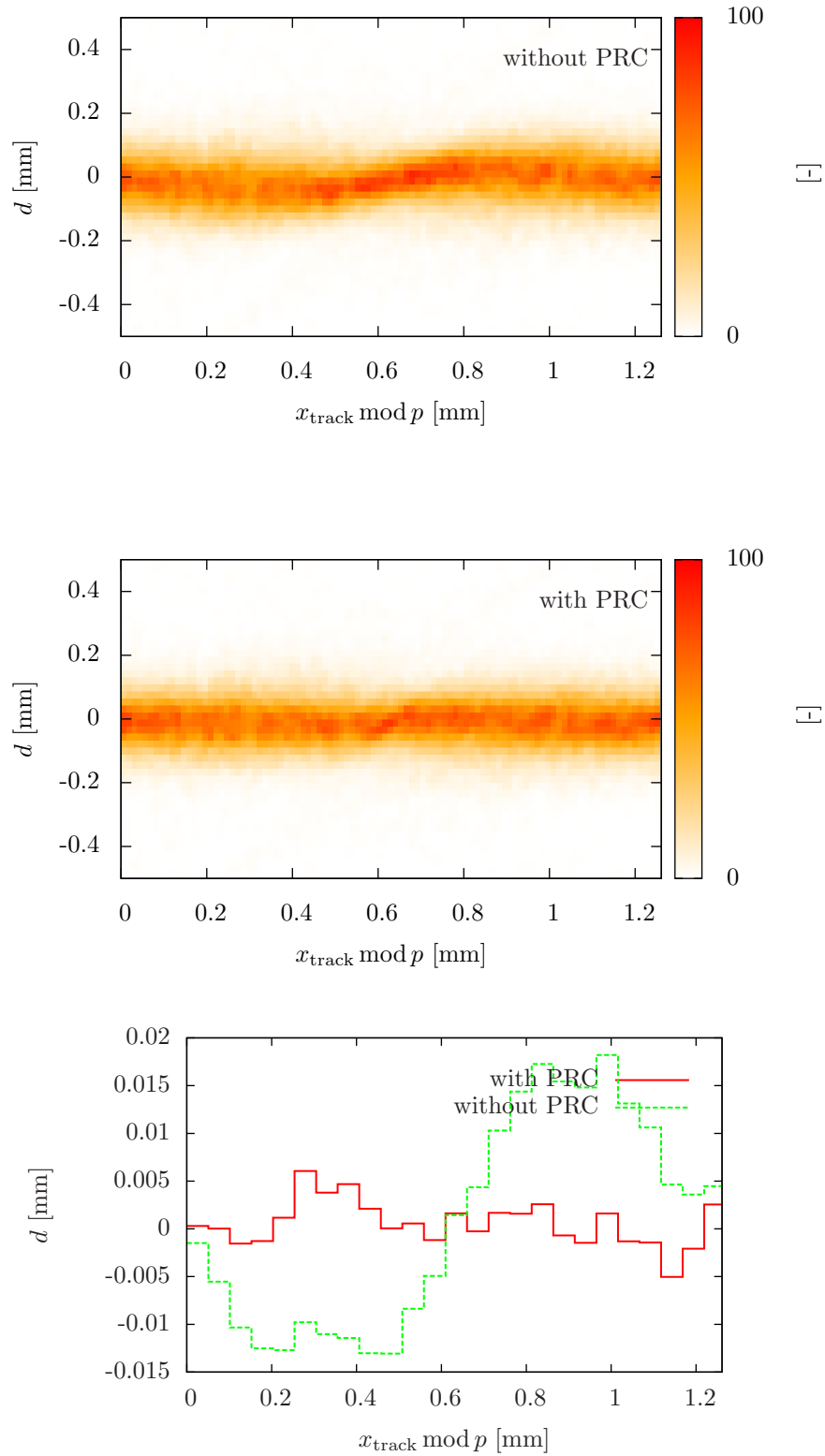


Figure 24: PRC quality plot for small pads and track angle $|\phi| < 0.02$ rad; two dimensional histogram of track position $x_{\text{track mod } p}$ and distance d for hits computed without and with PRC, plot of the mean distances from the upper diagrams

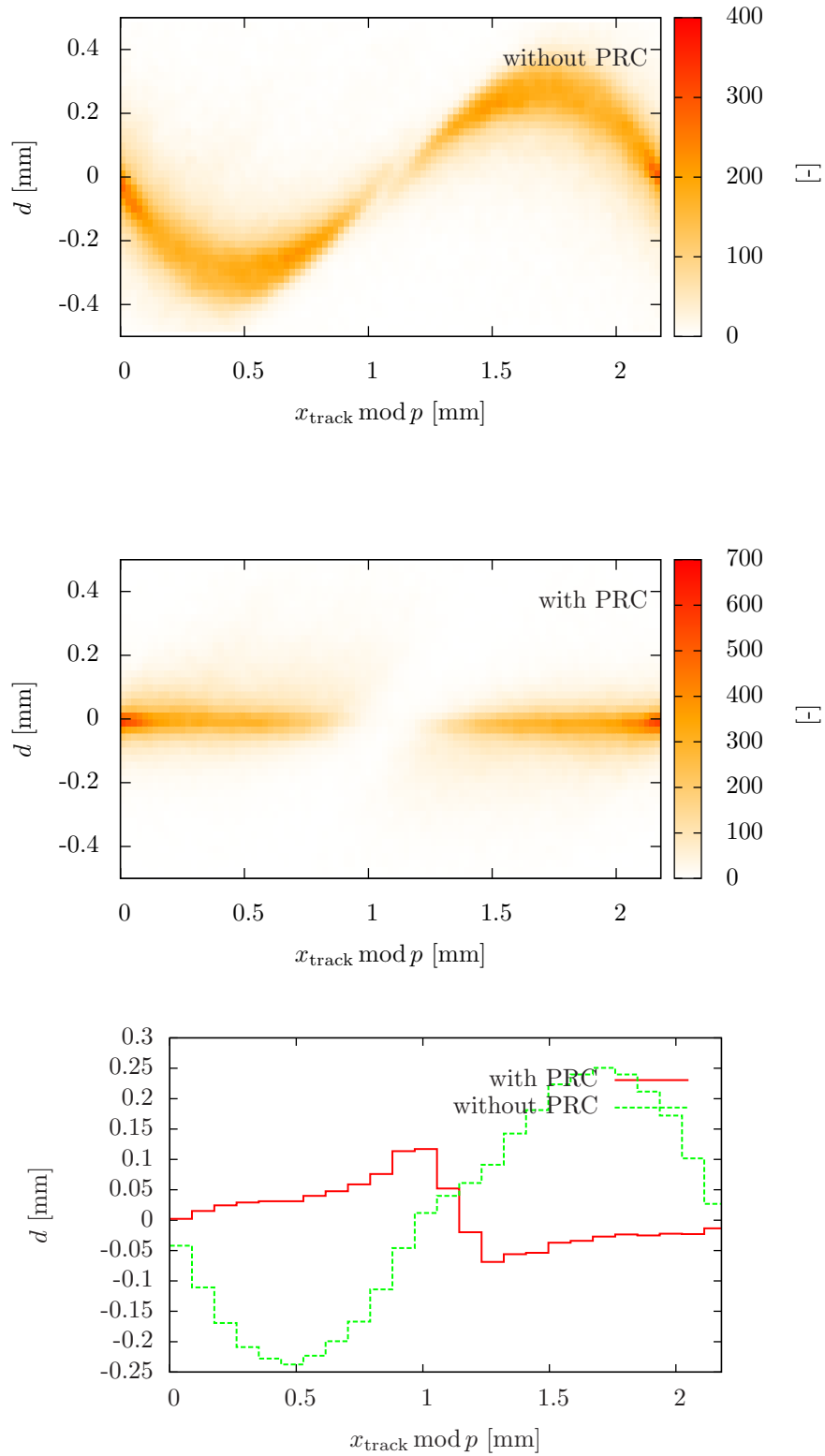


Figure 25: PRC quality plot for large pads; two dimensional histogram of track position $x_{\text{track mod } p}$ and distance d for hits computed without and with PRC, plot of the mean distances from the upper diagrams

The amplitude of the curve of the mean distances without PRC is roughly two orders of magnitude larger than in the case with small pads.

Even without the angle cut a clear reduction of the distances can be seen comparing the results with and without PRC. This observation corresponds with the analysis of the resolution in Sec. 4.2. There the PRC algorithm improves the resolution significantly for the 4 T run with large pads and hardly any improvement can be seen in case of the 3 T run with small pads.

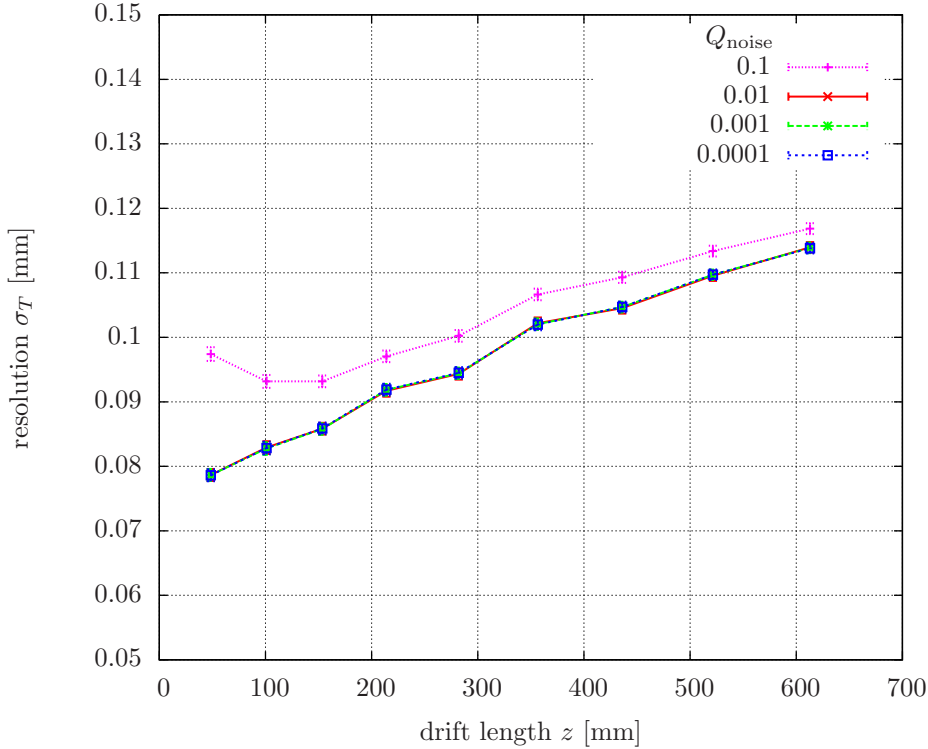


Figure 26: Resolution with small pads for different noise values

4.3.3 Noise Value

As described in Sec. 3.2.4.2 the coefficients essential for the PRC depend on the noise value Q_{noise} used in the simulation. The dependency of the point resolution of the tracks fitted with PRC on the noise value is examined in this section.

Running the simulation with different noise values provides the coefficients summarized in Tab. 4.

It has to be noticed that the coefficients for a noise value of $Q_{\text{noise}} = 0.001$ in Tab. 2 and Tab. 4 differ. This is due to a older ROOT version used to compute the coefficients in Tab. 2.

For all the previously presented examinations, except the results presented in this section, the values from Tab. 2 have been used. These were hard coded in the MultiFit source code. For the analysis in this section MultiFit has been modified to be able to read the coefficients for the PRC from a configuration file.

This feature is used to evaluate how the noise value affects the point resolution of the fitted tracks. This is carried out for the four noise values listed in Tab. 4 for the 4 T run with small pads using a χ^2 fit with PRC³¹. The results are shown in fig 26.

For the noise values Q_{noise} of 0.01, 0.001 and 0.0001 the resolution is practically identical. Only for a value of 0.1 the resolution is affected in a negative way.

Because of these results the effects of the PRC on the resolution can be regarded as independent of the noise value for realistic choices of this value.

³¹This is the only algorithm depending on the noise value.

$Q_{\text{noise}} = 0.0001$						
b_1	$a_{15} [-]$ -754.232	$a_{14} [-]$ 1770.85	$a_{13} [-]$ -1604.75	$a_{12} [-]$ 686.671	$a_{11} [-]$ -132.101	$a_{10} [-]$ 8.82685
b_2	$a_{25} [-]$ 1373.76	$a_{24} [-]$ -3301.41	$a_{23} [-]$ 3087.7	$a_{22} [-]$ -1385.5	$a_{21} [-]$ 290	$a_{20} [-]$ -21.1134
c_0	$a_{01} [-]$ 0.5002	$a_{00} [-]$ 0.128843				
c_2	$a_{26} [-]$ -4.28379					

$Q_{\text{noise}} = 0.001$						
b_1	$a_{15} [-]$ -862.766	$a_{14} [-]$ 1950.84	$a_{13} [-]$ -1715.1	$a_{12} [-]$ 717.037	$a_{11} [-]$ -135.612	$a_{10} [-]$ 8.935
b_2	$a_{25} [-]$ 1683.6	$a_{24} [-]$ -3865.35	$a_{23} [-]$ 3482.11	$a_{22} [-]$ -1517.69	$a_{21} [-]$ 311.179	$a_{20} [-]$ -22.4087
c_0	$a_{01} [-]$ 0.497417	$a_{00} [-]$ 0.155478				
c_2	$a_{26} [-]$ -0.615464					

$Q_{\text{noise}} = 0.01$						
b_1	$a_{15} [-]$ -877.501	$a_{14} [-]$ 1706.52	$a_{13} [-]$ -1274.67	$a_{12} [-]$ 441.417	$a_{11} [-]$ -62.7561	$a_{10} [-]$ 2.05507
b_2	$a_{25} [-]$ 1420.63	$a_{24} [-]$ -2771.44	$a_{23} [-]$ 2132.96	$a_{22} [-]$ -797.558	$a_{21} [-]$ 137.026	$a_{20} [-]$ -6.84216
c_0	$a_{01} [-]$ 0.495389	$a_{00} [-]$ 0.198754				
c_2	$a_{26} [-]$ 2.8563					

$Q_{\text{noise}} = 0.1$						
b_1	$a_{15} [-]$ 29166.5	$a_{14} [-]$ -68242.9	$a_{13} [-]$ 63622.5	$a_{12} [-]$ -29617	$a_{11} [-]$ 6897.16	$a_{10} [-]$ -642.032
b_2	$a_{25} [-]$ -63344.2	$a_{24} [-]$ 148373	$a_{23} [-]$ -138388	$a_{22} [-]$ 64381.8	$a_{21} [-]$ -14965.1	$a_{20} [-]$ 1391.03
c_0	$a_{01} [-]$ 0.49346	$a_{00} [-]$ 0.317525				
c_2	$a_{26} [-]$ 6.19218					

Table 4: Coefficients of the PRC algorithm for different noise values Q_{noise}

5 Results and Outlook

For large magnetic fields – in this case 3 T – the small pads improve the resolution considerably compared to large pads.

The data with small pads shows only little differences in the resolution between the different fit algorithms and their variations. Especially there is no positive effect of the PRC algorithm for drift distances z larger than 200 mm.

Nevertheless the quality analysis showed positive effects of the PRC for small angles. Consequently the PRC performance might be improved by taking into account the angle of the track during the correction of the hit position.

The resolution of the fit with PRC is not affected by the chosen noise value Q_{noise} for a large range of noise values. There is only an effect for very high noise values.

While all analysis in this work was performed using a non-staggered pad layout, a staggered pad plane is in preparation and will be tested in the next months.

References

- [1] Leo, W. R.: *Techniques for Nuclear and Particle Physics Experiments: A How-to Approach*. Springer-Verlag, Berlin, Heidelberg, New York, 1994
- [2] Lohse, T., Witzeling, W.: The Time Projection Chamber. *Instrum. in High Energy Phys.*, 81 (1992)
- [3] Nygren, D. R.: The Time Projection Chamber. *PEP Summer Study* PEP-0198 (1975)
- [4] Gluckstern, R. L.: Uncertainties in track momentum and direction, due to multiple scattering and measurement errors. *Nucl. Instrum. Meth.* **24**, 381 (1963)
- [5] Sauli, F.: GEM: A new concept for electron amplification in gas detectors. *Nucl. Instrum. Meth. A* **386**, 531 (1997)
- [6] Diener, R.: *Study of Reconstruction Methods for a Time Projection Chamber with GEM Gas Amplification System*. DESY-THESIS-2006-040, 2006
- [7] Janssen, M. E.: *Auflösungsstudien an einer Zeit-Projektions-Kammer (TPC) mit GEM Gasverstärkungssystem*. DESY-THESIS-2004-049, 2004
- [8] Janssen, M. E.: *Performance Studies of a Time Projection Chamber at the ILC*. DESY-THESIS-2008-011, 2008
- [9] Barlow, R.: *Statistics: A guide to the Use of Statistical Methods in the Physical Sciences*. John Wiley & Sons Ltd., Baffins Lane, Chichester, 1999
- [10] Carnegie, R. K., et al.: Resolution studies of cosmic-ray tracks in a TPC with GEM readout. *Nucl. Instrum. Meth. A* **538**, 372 (2005)
- [11] Behnke, T., et al.: LCIO - A persistency framework for linear collider simulation studies. <http://lcio.desy.de> (2008-09-08)
- [12] Brun, R., Rademakers, F.: ROOT - An Object Oriented Framework For Large Scale Data Analysis. <http://root.cern.ch> (2008-09-08)
- [13] Sauli, F.: *Principles of Operation of Multiwire Proportional and Drift Chambers*. CERN 77-09, 1977
- [14] Veenhof, R.: Garfield - simulation of gaseous detectors. <http://www.cern.ch/garfield> (2008-09-08)